# Optimizing the Dynamics of a Two-cell DC-DC Buck Converter by Time Delayed Feedback Control[☆]

M. Feki[a], A. El Aroudi[b,*], B. G. M. Robert[c], L. Martínez-Salamero[b]

[a] *Research Unit ICOS, Engineering School of Sfax, Sfax, Tunisia*
[b] *Universitat Rovira i Virgili, Departament d´Enginyeria Electrònica, Elèctrica i Automàtica, Tarragona, Spain*
[c] *Laboratoire CReSTIC, Université de Reims-Champagne-Ardenne, Reims, France*

**Abstract**

A study of the dynamical behavior of a two-cell DC-DC buck converter under a digital time delayed feedback control (TDFC) is presented. Various numerical simulations and dynamical aspects of this system are illustrated in the time domain and in the parameter space. Without TDFC, the system may present many undesirable behaviors such as sub-harmonics and chaotic oscillations. TDFC is able to widen the stability range of the system. Optimum values of parameters giving rise to fast response while maintaining stable periodic behavior are given in closed form. However, it is detected that in a certain region of the parameter space, the stabilized periodic orbit may coexist with a chaotic attractor. Boundary between basins of attraction are obtained by means of numerical simulations.

*Keywords:* Switching converters, Two-cell buck converter, TDFC,

[☆]This work is done within a Tunisian-Spanish cooperation framework under grant A/021698/08. Spanish MED funds under grant TEC-2007-67988-C02-01&2 are also acknowledged.

[*]Corresponding author
*Email address:* abdelali.elaroudi@urv.cat (A. El Aroudi)

Bifurcations, Modeling, Attractors coexistence
*2010 MSC:* 05.45.-a, 05.45.Gg, 05.45.Pq, 84.30.Jc

## 1. Introduction

Since the middle of the last century, electrical power has become the most appealing power due to its easiness to be used in industrial as well as residential environments [1, 2]. Therefore, the need to develop ways to convert and transmit this kind of power has drawn the interest of several researchers. During the last few decades, power electronics has undergone a boosting development in many aspects of technology, including power devices, circuit design, control methods and computer-aided analysis [3]. The main focus in power electronics circuit design remains the fulfilment of the functional requirements of the application for which the circuit has been designed. Power electronics converters have been widely used for more than three decades. During this period, several unusual strange behaviors have been observed (*e.g.* subharmonic oscillations, bifurcations and chaos) [4, 5] but very often they have been avoided by adjusting component values and parameters or by adding auxiliary security circuits [6, 7]. During the last two decades, tools for analyzing bifurcations and chaos have been well developed [8, 9], therefore, making the investigation of their very peculiar aspect an attractive endeavor [10, 11, 12].

Analysis, characterization and modeling of simple switching converters are still actively pursued today [13, 14]. It has been discovered that despite their simplicity, power converters are copious in nonlinear dynamics. This property is owed to toggling between a set of linear or nonlinear circuit

topologies, under the control of a feedback control system. Therefore, the control method as well as the circuit topology directly influence the dynamical behavior of the power converter [15].

Simple DC-DC converters, in all their simple types: buck, buck-boost and boost, have been thoroughly studied in recent years and different types of bifurcations have been perceived [9]. More recently, there has been an interest in analyzing the nonlinear behavior of the multi-cell power electronic converters [18, 19]. As a matter of fact, multi-cell power converters have been widely used in real applications since they circumvent shortcomings of ordinary switching devices due to their ability to support high voltages [20]. Recently, a two-cell buck converter has been also proposed for efficient wide-bandwidth envelope tracking in radio frequency power amplifiers [21]. It has been shown that chaotic behavior in these systems usually emerges from bad tuning of the feedback gain while trying to eliminate the static error by increasing this gain.

With the purpose to avoid the chaotic behavior in nonlinear systems and maintaining stable periodic regime, researchers tried to apply some techniques for controlling chaos [22]. The principle of these control methods is based on adding an extra input (preferably low energy signal) to the nonlinear system with the aim to modify its dynamics by stabilizing the desired behavior. The control input can be either a certain physical action on the system such as a force in a mechanical system or an external voltage in an electrical circuit or either a variation of some parameter of the controlled system in terms of its state variables trajectory in the state space [23].

One of the most efficient chaos control scheme is the Time Delay Feedback

Control (TDFC) first introduced by Pyragas [24] and later applied by many other authors. Roughly speaking, the time delayed scheme adds a control input which uses the difference between the feedback signal and its delayed version. In feedback systems, this input is added in the feedback path. If the time delay is selected to be the period of the Unstable Periodic Orbit (UPO), the latter can be stabilized by appropriately choosing the time delay feedback gain. A very important property of this control scheme is that it is a noninvasive control in the sense that the desired behavior of the system is not modified under the action of the TDFC and it is only stabilized. This method has been successfully applied to the elementary DC-DC buck converter [25], [26]. However, its main drawback is its difficulty to be implemented in analog hardware because of the requirement of a continuous memory during one delayed period. A possible solution to this problem is by using a digital TDFC. For this purpose, an accurate discrete time model must be derived for the system in order to be able to study the performances of the system under the digital TDFC [27, 28].

The aim of this work is to use a map that describes the nonlinear dynamical behavior of a two-cell DC-DC buck converter in order to design a TDFC that can achieve stable dynamics within a wide range of the design parameter space. As it will be shown later, the application of the TDFC technique is a powerful strategy for avoiding subharmonic oscillations and chaotic behavior while widening the stability region in the design parameter space.

The rest of the paper is outlined as follows. In the next section, we present a complex discrete model of the converter issued from the solutions

of the continuous time equations and we present next the simplified model. Then, we present a series of numerical simulations of the obtained models. Section three will be devoted to analyzing the effect of adding TDFC. Both linear stability analysis, based on Jacobian matrix, and nonlinear stability analysis, based on a Lyapunov function, led to similar results. Coexistence of attractors are detected from numerical simulations in the same section and some explanations of this phenomenon are given. Finally, the last section will include the concluding remarks and the perspectives.

## 2. Modeling the two-cell DC-DC converter

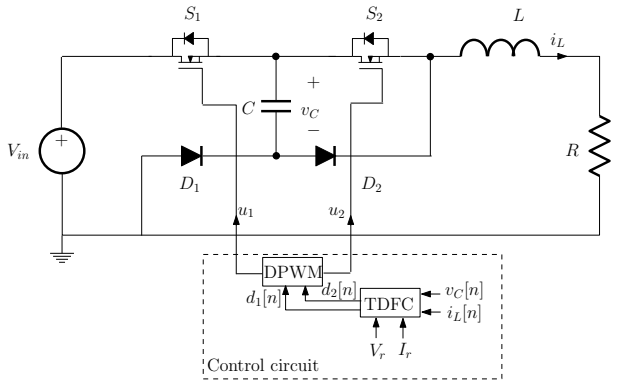


Figure 1: A basic two-cell DC-DC buck converter with an RL load and its control circuit. $S_i$ and $D_i$ are the switch and diode of the $i^{th}$ cell, the capacitor $C$ ensures voltage balance between cells, $V_{in}$ is the supply voltage, $v_C$ and $i_L$ are the circuit states and $u_k$ is the DPWM output signal with duty cycle $d_k$.

The converter that we will deal with in this paper is depicted in Figure 1. It is based on a buck chopper (see [1]) modified in order to allow a higher input voltage by using two serial switches (transistors and diodes) [18, 19, 20]. The role of the capacitor is to balance the switch voltages. The signals $u_1$ and

$u_2$ are the outputs of a digital pulse width modulator (DPWM) driven by a feedback control system to be designed in later sections to achieve a constant average value of $v_C = \frac{V_{in}}{2}$ and a constant averaged value of the output current $i_L$ equal to a reference current $I_r$. The control signals are the duty cycles $d_1$ and $d_2$ of the driving signal used for the switches $S_1$ and $S_2$. It is worth noting that in this work, we will define the duty cycles with respect to the OFF state rather than the ON state. Therefore the switch $S_k$ will remain in its OFF state during $d_k T$ when it is driven by a driving signal $u_k(t)$ with a duty cycle $d_k$. We also notice that the duty cycle $d_k$ cannot exceed unity neither can it go beyond zero, thus when calculated $d_k$ may undergo upper or lower saturation if the obtained value is not in the unit interval.

In a typical operating mode, because of the continuity of the inductor current and due to the natural turn off switching of diodes under negative voltages, the switch $S_k$ and the diode $D_k$ are always turned ON and OFF in a complementary manner. Under a fixed frequency PWM control, when the switch $S_k$ is closed, the diode $D_k$ is open and vice versa. As we have two switches $S_1$ and $S_2$, then we can easily define four different operating topologies, (see Table 1). By applying Kirchhoff laws to the two-cell converter, the following switched model is obtained:

$$\frac{d}{dt}\begin{pmatrix} i_L \\ v_C \end{pmatrix} = \begin{pmatrix} -\frac{R}{L} & (u_2 - u_1)\frac{1}{L} \\ (u_1 - u_2)\frac{1}{C} & 0 \end{pmatrix}\begin{pmatrix} i_L \\ v_C \end{pmatrix} + \begin{pmatrix} \frac{V_{in}}{L} u_1 \\ 0 \end{pmatrix} \tag{1}$$

where $u_k$ are the driving signals for the switches $S_k$ given by:

$$u_k = \begin{cases} 1 & \text{if} \quad S_k \quad \text{is closed (ON)} \\ 0 & \text{if} \quad S_k \quad \text{is open (OFF)} \end{cases} \tag{2}$$

Six different operating modes are possible depending on the values of the duty cycles $d_1$ and $d_2$. The driving signals corresponding to these operating modes are depicted in Figure 2.

Table 1: Two-cell DC-DC converter different topologies between which toggling occurs

| Topologies | state of $S_1$ | state of $S_2$ |
|---|---|---|
| Topology 1 ($\mathcal{T}_1$) | OFF | ON |
| Topology 2 ($\mathcal{T}_2$) | ON | ON |
| Topology 3 ($\mathcal{T}_3$) | ON | OFF |
| Topology 4 ($\mathcal{T}_4$) | OFF | OFF |

### *2.1. Obtaining the discrete time model*

Toggling between different topologies occurs according to the values of the duty cycles $d_1$ and $d_2$ at the beginning of the PWM period $T$. Figure 3 shows the form of steady state the driving signals $u_1$ and $u_2$ together with the their corresponding system response in terms of the state variables $i_L$ and $v_C$.

As a matter of fact, we can define several different toggling modes, to each of which we can assign a recurrent system to express the values of the states at the end of the period in terms of the values at the beginning of the period. Once at $T-$periodic steady state, only one recurrent function will represent the behavior of the converter. However, during the transient phase, the duty cycles may saturate and may assume any value depending on the control system and therefore different periods might be governed by various modes. The two-cell converter can be described by the following switched mode model:

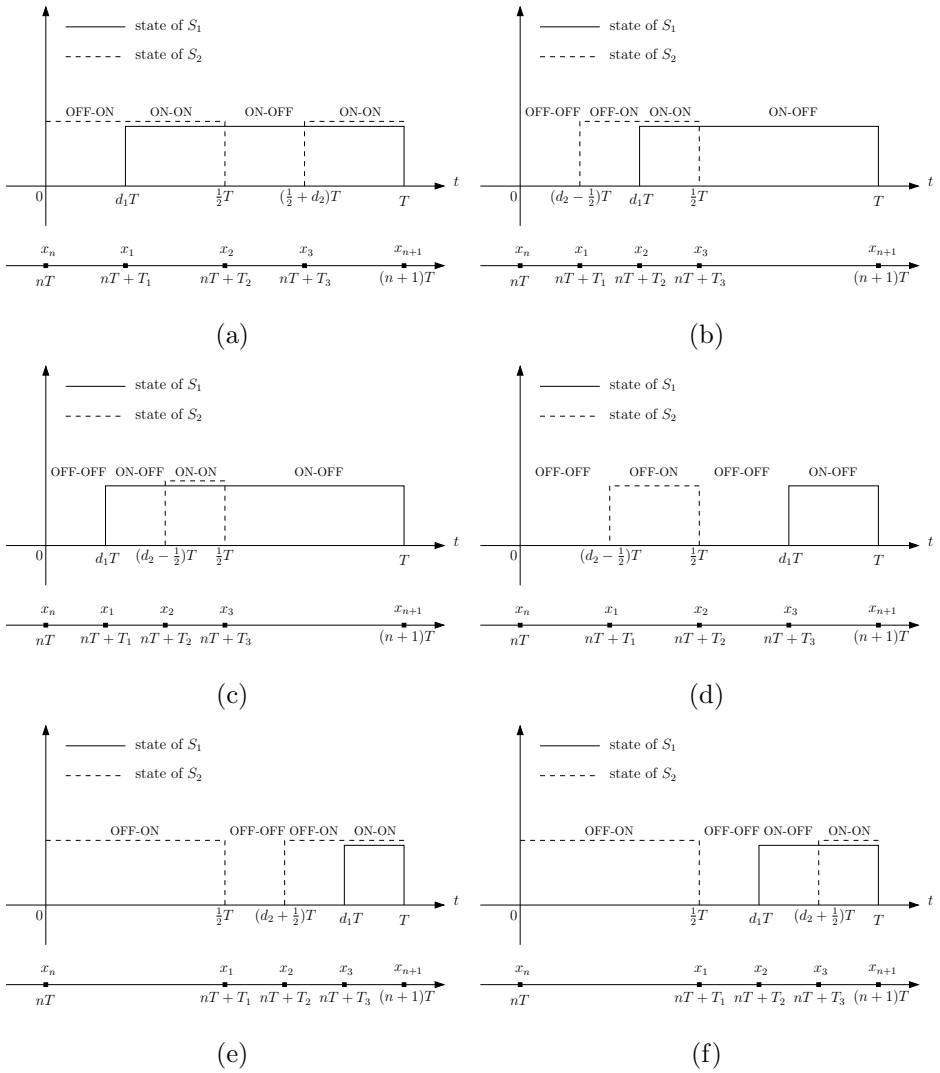


Figure 2: Different possible operating modes for the two-cell DC-DC buck converter. (a) Mode 1: $d_1 < \frac{1}{2}$ and $d_2 < \frac{1}{2}$, (b) Mode 2: $d_1 < \frac{1}{2}$ and $0 < d_2 - \frac{1}{2} < d_1$, (c) Mode 3: $d_1 < \frac{1}{2}$ and $d_1 < d_2 - \frac{1}{2} < \frac{1}{2}$, (d) Mode 4: $d_1 > \frac{1}{2}$ and $d_2 > \frac{1}{2}$, (e) Mode 5 $\frac{1}{2} < d_2 + \frac{1}{2} < d_1$, (f) Mode 6: $d_1 < d_2 + \frac{1}{2} < 1$ and $\frac{1}{2} < d_2 + \frac{1}{2} < d_1$

$$\begin{aligned} \dot{x} &= A_1 x + B_1 \quad \text{during} \quad [t_0, t_1] \\ \dot{x} &= A_2 x + B_2 \quad \text{during} \quad [t_1, t_2] \\ \dot{x} &= A_3 x + B_3 \quad \text{during} \quad [t_2, t_3] \\ \dot{x} &= A_4 x + B_4 \quad \text{during} \quad [t_3, t_4] \end{aligned} \tag{3}$$

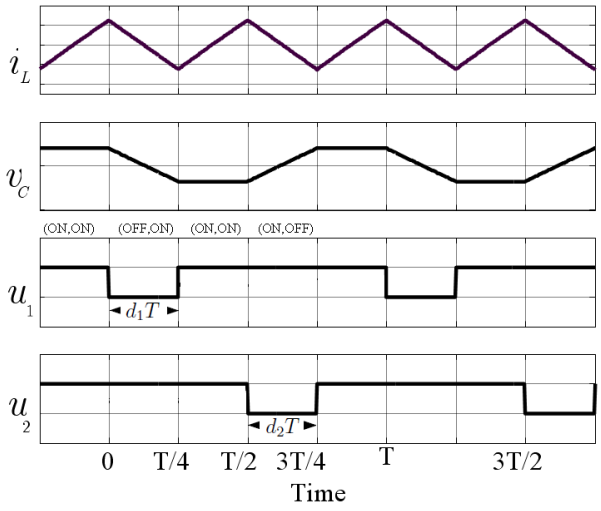


Figure 3: Driving signals $u_1$ and $u_2$ and the state variables $i_L$ and $v_C$ of a basic two-cell DC-DC buck converter in steady state periodic behavior.

where $A_k$ and $B_k$ can be easily deduced from the switched model (1) by specifying the operating mode and giving values to the driving signal $u(t)$, $t_k$ ($k = 1 \ldots 4$) are the switching instants, being $t_0 = nT$, $t_4 = (n+1)T$ and ($t_1$, $t_2$ and $t_3$) decided by the controller (See Fig. 2). Eq (3) is piecewise linear and taking advantage of the linearity of the system during each switching interval, the solution during this interval can be written as follows [16]

$$x(t) = e^{A_k(t-t_k)}x(t_k) + \int_{t_k}^{t} e^{A_k(t-\tau)}B_k d\tau \tag{4}$$

By stacking-up the solutions, the following model is obtained [18]:

$$x[n+1] = \mathbf{\Phi}(\mathbf{d}[n])x[n] + \mathbf{\Psi}(\mathbf{d}[n]) \tag{5}$$

where $x[n] = x(nT)$, $x[n+1] = x((n+1)T)$ and

$$\mathbf{d}[n] = (d_1[n], d_2[n])^t \tag{6}$$

$$\mathbf{\Phi}(\mathbf{d}[n]) = \phi_4\phi_3\phi_2\phi_1 \tag{7}$$

$$\mathbf{\Psi}(\mathbf{d}[n]) = \phi_4\phi_3\phi_2\psi_1 + \phi_4\phi_3\psi_2 + \phi_4\psi_3 + \psi_4 \tag{8}$$

$$\phi_k = e^{A_k\delta t_k} \text{ and } \psi_k = \int_{t_k}^{t_{k+1}} e^{A_k(t-\tau)}B_k d\tau \tag{9}$$

where $\delta t_k = t_{k+1} - t_k$ is the lapse of time between two consecutive switching instants. As it can be noticed, this model is extremely complicated to handle from a theoretical analysis point of view. In order to simplify the nonlinear model of the system while maintaining practical considerations, we will assume some realistic assumptions with the purpose of obtaining an affine expression in the control signals $d_1$ and $d_2$. We will proceed by approximating the entries of the matrix exponential $e^{At}$ by using Taylor's expansion to the first order. This is possible since the time durations between switchings are much smaller than time constant of the system and the state variables can therefore be considered practically piecewise linear. Therefore, it can be written

$$e^{A_k t} \simeq \mathbb{I} + A_k t + \mathcal{O}((A_k t)^2) + \ldots \tag{10}$$

With the above consideration, it can be demonstrated that all the above operating modes can be described by the following simplified model [30]

$$x[n+1] = (\mathbb{I} + AT)x[n] + BT \tag{11}$$

where

$$A = \sum_{k=1}^{4} A_k\delta t_k, \;\; B = \sum_{k=1}^{4} B_k\delta t_k \tag{12}$$

Now by substituting $A_k$, $B_k$ and $\delta t_k$ by their expressions, we obtain

$$\begin{pmatrix} i_L[n+1] \\ v_C[n+1] \end{pmatrix} = \begin{pmatrix} 1-\frac{TR}{L} & (d_1[n]-d_2[n])\frac{T}{L} \\ (d_2[n]-d_1[n])\frac{T}{C} & 1 \end{pmatrix} \begin{pmatrix} i_L[n] \\ v_C[n] \end{pmatrix} \tag{13}$$

$$+ \begin{pmatrix} \frac{V_{in}T}{L}(1-d_1[n]) \\ 0 \end{pmatrix} \tag{14}$$

For the sake of reducing the number of parameters of the system we will consider some new dimensionless variables, where the current is normalized by the maximum current in the circuit, the voltage is normalized by the maximum voltage and time is normalized by the switching period. If we let $\delta_L = \frac{RT}{L}$, $\delta_C = \frac{T}{RC}$, $x_i[n] = \frac{Ri_L[n]}{V_{in}}$ and $x_v[n] = \frac{v_C[n]}{V_{in}}$, we obtain the following dimensionless model

$$\begin{pmatrix} x_i[n+1] \\ x_v[n+1] \end{pmatrix} = \begin{pmatrix} 1-\delta_L & (d_1[n]-d_2[n])\delta_L \\ (d_2[n]-d_1[n])\delta_C & 1 \end{pmatrix} \begin{pmatrix} x_i[n] \\ x_v[n] \end{pmatrix} + \begin{pmatrix} \delta_L(1-d_1[n]) \\ 0 \end{pmatrix} \tag{15}$$

In this section we present some numerical simulations with a simple proportional control strategy. Herein, the duty cycles are calculated on the basis of

$$d_1[n] = k_i(x_i[n]-I_r) + k_v(x_v[n]-V_r) \tag{16}$$

$$d_2[n] = k_i(x_i[n]-I_r) - k_v(x_v[n]-V_r) \tag{17}$$

where $k_i$ and $k_v$ are the proportional gains of the current and voltage errors respectively. We implicitly understand from any expression of the duty cycles $d_1$ and $d_2$ that it undergoes a saturation because during one switching period

the OFF time can not be bigger than this period neither negative. Therefore, the applied duty cycle is in fact $\mathrm{sat}(d_k)$ and not $d_k$, where $\mathrm{sat}(d)$ is the function defined by:

$$\mathrm{sat}(d) = \frac{1}{2}\left(1 + |d| - |d-1|\right) \tag{18}$$

and the actual duty cycles become

$$\begin{pmatrix} d_1[n] \\ d_2[n] \end{pmatrix} = \mathrm{sat}\left(\begin{pmatrix} k_i & k_v \\ k_i & -k_v \end{pmatrix}\begin{pmatrix} x_i[n] - I_r \\ x_v[n] - V_r \end{pmatrix}\right) \tag{19}$$

which can be written in a more compact form as $\mathbf{d}[n] = \mathrm{sat}(K(x[n] - X_r))$, where $x[n] = (x_i[n],\ x_v[n])^t$, $X_r = (I_r,\ V_r)^t$ and

$$K = \begin{pmatrix} k_v & k_i \\ k_v & -k_i \end{pmatrix} \tag{20}$$

Due to the piecewise aspect of the duty cycles, we can easily verify that the system can mathematically have several fixed points. However, only the non saturated fixed point has a practical interest. The expression of this fixed point will be given later.

### *2.2. Model Verification from Numerical simulations*

In the previous section, we have presented different models of the two-cell DC-DC buck converter. The first is the exact model (1) which is not appropriate to deal mathematically with it. Indeed, the model that represents the overall dynamics of the converter is a non-autonomous switched and non affine in the control signal. Therefore, the only use of this complex model is to check via numerical simulations whether any suggested control strategy would be efficient or not on the exact model, which gives a closer idea to

the reality. The second model (5) is the exact discrete time model which has the advantage of carrying out fast numerical simulations but it presents the same shortcoming of the switched model in terms of mathematical treatment. The third model (15) which comes from tenable simplification of the exact discrete time model presents several advantages. First of all, the model is unique for all operating continuous conduction mode[1]. Second, the obtained model is simple making its analysis easier.

*2.2.1. Simulating the simple model*

The normal periodic running mode of the controlled converter, which is the period-one mode, corresponds to the fixed point of the recurrent relation (15) together with (16)-(17). The fixed point denoted by $(x_i^*, x_v^*)$ is obtained by solving $(x_i[n+1], x_v[n+1]) = (x_i[n], x_v[n])$. This yields to

$$(x_i^*, x_v^*) = \left( \frac{1 + k_i I_r}{1 + k_i}, V_r \right) \tag{21}$$

It is clear that while, under mild conditions, the reference voltage will be attained, the reference current can only be approached from above when $k_i$ is very large. Mathematically written

$$\lim_{k_i \to \infty} x_i^* = I_r^+ \tag{22}$$

An in-depth analysis of conditions on the stability of the closed loop system will be elucidated in the next section.

The chaotic behavior is well delineated using the bifurcation diagram of Figure 4(a)-(b). The parameters used for the power circuit are the following:

[1]The inductor current never drops to zero.

$\delta_C = \delta_L = 0.1$ such that the switching period $T$ is small compared to the circuit time constants, $I_r = 0.6$ is arbitrarily chosen and $V_r = \frac{1}{2}$ since it is required that $v_C = \frac{V_{in}}{2}$. The curves in red represent the current values at which the duty cycle saturates. Since at steady state we have $x_v[n] = V_r$ for all $k_i$, then (16) and (17) imply that $d_1[n] = d_2[n]$ and hence both duty cycles have similar upper and lower saturation limits, hereafter called boundaries (represented in red). These limits occur when $d_k[n] = 1$ and when $d_k[n] = 0$ that is

$$d_k[n] = 1 \quad \Leftrightarrow \quad x_{i,sat,upper} = \frac{1}{k_i} + I_r \tag{23}$$

$$d_k[n] = 0 \quad \Leftrightarrow \quad x_{i,sat,lower} = I_r \tag{24}$$

*2.2.2. Simulating the complete model*

The fixed point of the complete accurate model is obtained from the equation: $x^* = \mathbf{\Phi}(\mathbf{d}[n])x^* + \mathbf{\Psi}(\mathbf{d}[n])$ which implies that: $x^* = [(\mathbb{I} - \mathbf{\Phi}(\mathbf{d}^*)]^{-1}\mathbf{\Psi}(\mathbf{d}^*)$ provided that $[(\mathbb{I} - \mathbf{\Phi}(\mathbf{d}^*)]^{-1}$ is a nonsingular matrix. Therefore, in the case of the complete model, we have no hope in solving this set of equations analytically to obtain the fixed point $x^*$ because $\mathbf{d}^*$ is imposed by the controller to depend on $x^*$ as $\mathbf{d}^* = K(x^* - X_r)$. Therefore, we will only present numerical simulations with similar controller parameters so comparison can be held.

When the proportional gains are fixed to obtain normal operating behavior (period-one behavior), numerical simulations have shown that the simple model and the accurate model have very similar responses (compare Figure 4(a) with Figure 4(c) and Figure 4(b) with Figure 4(d)). According to the bifurcation diagrams, the bifurcation of the solution (from period-one to period-two) occurs when $k_i = 19$ for the simple model, however with the

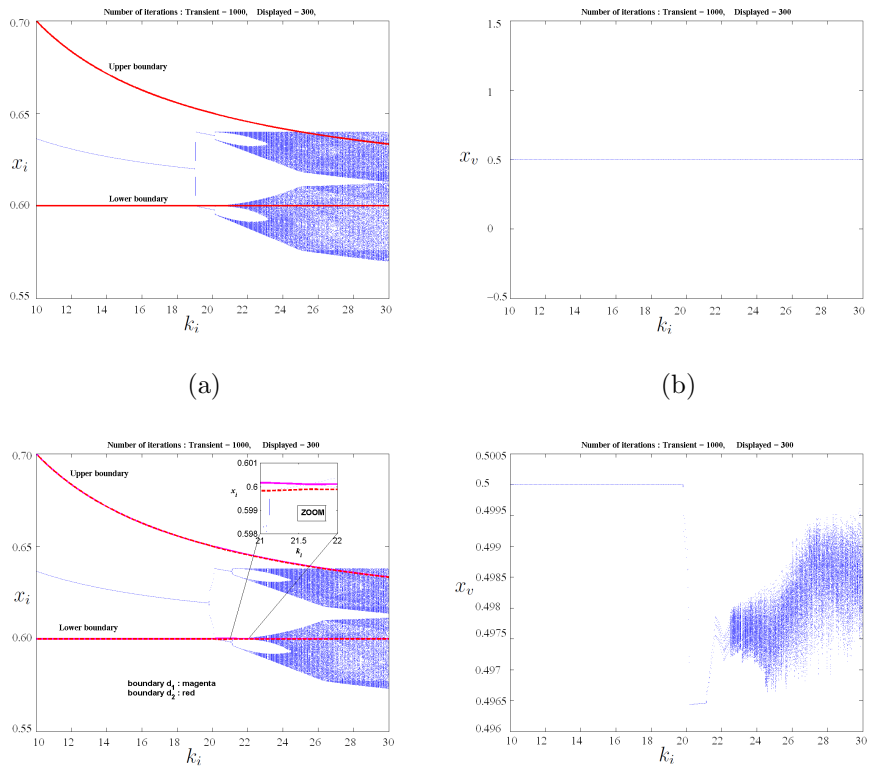


Figure 4: Bifurcation diagrams of $x_i$ and $x_v$ of the exact and simplified models with respect to bifurcation parameter $k_i$. (a) Inductor current of the simplified model. (b) Capacitor voltage of the simplified model. (c) Inductor current of the exact model. (d) Capacitor voltage of the exact model.

accurate model, the bifurcation occurs with larger value of $k_i \approx 19.8$. It is also worth to note that beyond the bifurcation value of $k_i$, there is no exact convergence of $v_C$ to $V_r$ (see Figure 4(d)), *i.e.*, we have also a chaotic behavior of the voltage which is practically more reasonable than having chaotic behavior of the current and stable behavior of the voltage as it has been obtained by the simple model. Consequently, calculating the boundaries in

terms of $k_i$ is not trivial and the boundary expressions depend on the error $(x_v - V_r)$. To hold the comparison over, we have sketched the boundaries with the average value of the error. Although, those boundaries have no pertinence, they may reveal explanation of some bifurcations as it can be seen in the zoomed part of Figure 4(c).

The comparison between the simulation results of the simple and the accurate models did not reveal a significant difference in the response. As a conclusion, we can consider the simple model for theoretical analysis and design, all along caring to check the performances of the suggested control method on the accurate model.

## 3. Time-delayed feedback control (TDFC)

Since we have noticed that, for the simple model, only the current behavior undergoes two bifurcations until it reaches chaos, then it is tenable to apply the TDFC part in terms of current only. Omitting the saturation, the duty cycle expressions with TDFC are

$$d_1[n] = k_i(x_i[n] - I_r) + k_v(x_v[n] - V_r) + \eta_i(x_i[n] - x_i[n-1]) \quad (25)$$

$$d_2[n] = k_i(x_i[n] - I_r) - k_v(x_v[n] - V_r) + \eta_i(x_i[n] - x_i[n-1]) \quad (26)$$

The application of the TDFC controller increases by one the order of the discrete dynamical system. It is worthy to note here that this is one great advantage of using a discrete model. When applying TDFC to a continuous-time dynamical system, the system becomes infinite dimensional. Let's assume

the following notations

$$x[n] = \begin{pmatrix} x_1[n] \\ x_2[n] \\ x_3[n] \end{pmatrix} = \begin{pmatrix} x_v[n] \\ x_i[n] \\ x_i[n-1] \end{pmatrix} \tag{27}$$

Then the closed loop system, obtained by applying (25) and (26) to (15), is described by the following recurrent map

$$\begin{aligned} x_1[n+1] &= x_1[n] - 2k_v\delta_C\big(x_1[n] - V_r\big)x_2[n] \\ x_2[n+1] &= 2k_v\delta_L\Big(x_1[n] - V_r - \tfrac{1}{2}\Big)x_1[n] + \big(1 - \delta_L(k_i + \eta_i + 1)\big)x_2[n] \\ &\quad + \delta_L\eta_i x_3[n] + \delta_L(1 + k_i I_r + k_v V_r) \\ x_3[n+1] &= x_2[n] \end{aligned} \tag{28}$$

The fixed point $x^*$ of the normal operating mode is obtained by equating $x^*[n+1] = x^*[n]$. Since this equation gives $x_3^* = x_2^*$, then the TDFC part will vanish and we obtain similar fixed point as in the previous section, that is

$$(x_1^*, x_2^*, x_3^*) = \left(V_r, \frac{1 + k_i I_r}{1 + k_i}, \frac{1 + k_i I_r}{1 + k_i}\right) \tag{29}$$

196 *3.1. Linear stability analysis*

Linearizing system (28) around its fixed point yields to the following Jacobian matrix

$$J = \begin{pmatrix} 1 - 2k_v\delta_C x_2 & -2k_v\delta_C(x_1 - V_r) & 0 \\ k_v\delta_L(2V_r - 1) & 1 - \delta_L(k_i + \eta_i + 1) & \delta_L\eta_i \\ 0 & 1 & 0 \end{pmatrix} \tag{30}$$

When substituting $x = x^*$ and $V_r = \frac{1}{2}$, the characteristic equation of the Jacobian matrix is

$$(\lambda - 1 + 2k_v\delta_C x_2^*)\left(\lambda^2 - \big(1 - \delta_L(k_i + \eta_i + 1)\big)\lambda - \delta_L\eta_i\right) = 0 \tag{31}$$

Clearly, $\lambda_1 = 1 - 2k_v\delta_C x_2^*$ is an eigenvalue for the system that we should place inside the unit circle of the complex plane by tuning the control gains $k_i$ and $k_v$ [16], [17]. Therefore, we have

$$|1 - 2k_v\delta_C x_2^*| < 1 \tag{32}$$

We finally may select $k_v$ as follows

$$0 < k_v < \frac{1}{\delta_C x_2^*} \tag{33}$$

To obtain a fast response, we may impose the eigenvalue to be at the origin [16], [17]. This can be achieved by choosing

$$k_v = \frac{1}{2\delta_C x_2^*} \tag{34}$$

For the quadratic part of (31), we may apply Jury's criterion of stability (see [16]) that requires the following conditions to be satisfied

$$| a_0 | < 1 \tag{35}$$

$$1 + a_1 + a_0 > 0 \tag{36}$$

$$1 - a_1 + a_0 > 0 \tag{37}$$

where

$$a_1 = -\big(1 - \delta_L(k_i + \eta_i + 1)\big) \tag{38}$$

$$a_0 = -\delta_L \eta_i \tag{39}$$

The above inequalities define several regions in the plane $k_i - \eta_i$. The region of stability is then the intersection between each defined region. Condition (35) gives

$$| \eta_i | < \frac{1}{\delta_L} \tag{40}$$

Condition (36) gives

$$k_i > -1 \tag{41}$$

which is satisfied when restricting the design to positive values of $k_i$ and finally (37) yields

$$\eta_i < -\frac{k_i}{2} + \frac{1}{\delta_L} - \frac{1}{2} \tag{42}$$

198 The intersection of the regions defined by the inequalities (40)-(42) is the shaded area depicted in Figure 5. We notice that the critical proportional

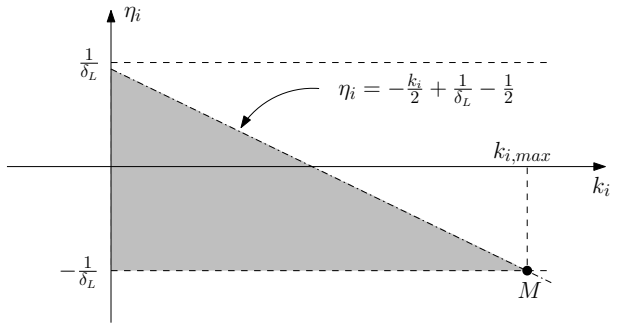


Figure 5: The stability zone in the parameter plane $k_i - \eta_i$.

199

200 gain $k_i$ can be made larger, and then the stability region can be enlarged,
201 by using a negative TDFC action ($\eta_i < 0$). However, we cannot increase the
202 current gain $k_i$ indefinitely. The intersection point $M$ in Fig. 5 defines the
203 maximum value of $k_i$ which is given by $k_{i,max} = \frac{4}{\delta_L} - 1$.

204 *3.2. Nonlinear stability analysis*

Similar results can be obtained using a nonlinear stability analysis. We should note that the stability analysis we will present herein only concerns the non saturating case. A thorough analysis including the saturation of the duty cycles will be included in future work. To tackle our analysis, we define

the error vector as $e_1[n] = x_1[n] - V_r$, $e_2[n] = x_2[n] - I_r$ and $e_3[n] = x_3[n] - I_r$ and thus we obtain the error system

$$\begin{aligned} e_1[n+1] &= \big(1 - 2k_v\delta_C x_2[n]\big)e_1[n] \\ e_2[n+1] &= 2k_v\delta_L\Big(e_1[n] - V_r - \tfrac{1}{2}\Big)e_1[n] + \big(1 - \delta_L(k_i + \eta_i + 1)\big)e_2[n] \\ &\quad +\delta_L\eta_i e_3[n] + \delta_L(1 - I_r) \\ e_3[n+1] &= e_2[n] \end{aligned} \tag{43}$$

we remark that the error system is a nonlinear system in a cascade triangular form

$$z_1[n+1] = f_1(z_1[n]) \tag{44}$$

$$z_2[n+1] = f_2(z_1[n], z_2[n]) \tag{45}$$

with $z_1 = e_1$ and $z_2 = [e_2, e_3]^t$. It has been proved that under mild conditions, the stability of system (44)-(45) can be deduced from the simultaneous asymptotic stability of the following subsystems [29]

$$z_1[n+1] = f_1(z_1[n]) \tag{46}$$

$$z_2[n+1] = f_2(z_1^*, z_2[n]) \tag{47}$$

where $z_1^*$ is the fixed point of (46). Now, the first subsystem is described by

$$e_1[n+1] = \big(1 - 2k_v\delta_C x_2[n]\big)e_1[n] \tag{48}$$

Hence, we may consider the Lyapunov function candidate $V(e_1[n]) = e_1[n]^2$. In discrete systems we need to show that the first difference of the Lyapunov function is negative *i.e.* $\Delta V(e_1[n]) = V(e_1[n+1]) - V(e_1[n]) < 0$.

$$\Delta V(e_1[n]) = 2k_v\delta_C x_2[n]\big(2k_v\delta_C x_2[n] - 2\big)e_1[n]^2 \tag{49}$$

Knowing that $x_2[n]$ is always positive, then we can guarantee that $\Delta V$ is negative if the voltage gain $k_v$ is chosen to satisfy condition (50).

$$0 < k_v < \frac{1}{\delta_C x_2[n]} = k_{v,cri} \tag{50}$$

We notice that condition (50) is equivalent to condition (33) around the fixed point. We can also optimize the choice of $k_v$ to obtain fast convergence of the error to zero. This is done by minimizing $\Delta V(e_1[n])$, therefore we need to minimize $h(k_v) = 2k_v\delta_C x_2[n]\big(2k_v\delta_C x_2[n] - 2\big)$ with respect to $k_v$ and we get

$$k_{v,opt} = \frac{1}{2\delta_C x_2[n]} \tag{51}$$

As it can be observed, this condition is the same than that given in (34) with the difference that (34) is obtained from the linear approach with $x_2[n]$ evaluated at the fixed point component $x_2^*$.

Until now, we can guarantee the stability of subsystem (48) at the origin by the choice of $k_v$, that is we obtain $e_1[n] = 0$ equivalent to $x_1[n] = V_r$. Now, by substituting $e_1[n] = 0$ in the second subsystem *i.e.* $z_2[n+1] = f_2(0, z_2[n])$ we get

$$\begin{aligned} e_2[n+1] &= \big(1 - \delta_L(k_i + \eta_i + 1)\big)e_2[n] + \delta_L\eta_i e_3[n] + \delta_L(1 - I_r) \quad (52)\\ e_3[n+1] &= e_2[n] \quad (53) \end{aligned}$$

This is a linear system with characteristic equation

$$\lambda^2 - \Big(1 - \delta_L(k_i + \eta_i + 1)\Big)\lambda - \delta_L\eta_i = 0 \tag{54}$$

which has been studied in the previous section. To summarize, the analysis carried out here, we can say that if we choose $k_v < \frac{1}{\delta_C}$ and any pair of $(k_i, \eta_i)$

in the shaded area of Fig. 5, then the system evolves towards the fixed point $(x_1^*, x_2^*, x_3^*)$. To obtain a fast evolution, we might prefer to choose $k_v = \frac{1}{2\delta_C}$ and choose the pair of $(k_i, \eta_i)$ that gives a minimum spectral radius that corresponds to eigenvalues of (54) with the least norm, that should be the pair that leads to equal real eigenvalues. The optimal value of $\eta_i$ verifies:

$$\eta_{i,opt} = -\frac{1 + \delta_L(1 + k_i) - 2\sqrt{\delta_L(1 + k_i)}}{\delta_L} \tag{55}$$

### *3.3. Simulation Results of the TDFC Performances*

In this section we present numerical simulations that confirm the theoretical results obtained in the foregoing section. Following the theoretical analysis presented earlier, we have shown that $k_v$ can be chosen to achieve $x_1 = V_r$, thus we have fixed $k_v = \frac{1}{2\delta_C} = 5$. Next, we will present simulations with different pairs of $(k_i, \eta_i)$.

First, in Fig. 6 we present the evolution of the current $x_2[n]$ and the voltage $x_1[n]$ with $k_i$ increased near to its maximum $k_{i,cri} = 38.5$ and $\eta_i = -9.85$ thus the obtained steady state error is about 1%. To investigate the optimality relation presented in (55) we present two different curves of the current with $k_i = 31$ while $\eta_i$ is fixed first at $\eta_i = -8$ and then at $\eta_i = \eta_{i,opt}$. The initial conditions where fixed at +5% of the fixed point values. The results are shown in Fig. 7. Clearly, the current settles to the steady state faster when using $\eta_{i,opt}$. To confirm the optimality relation, we present in Fig. 8 another simulation at $k_i = 25$.

Figure 9 depicts a 2D-bifurcation diagram where the behavior of the converter is elucidated for each pair of parameter $(k_i, \eta_i)$. This diagram is obtained from an ad hoc routine written in Matlab. The colors indicate different

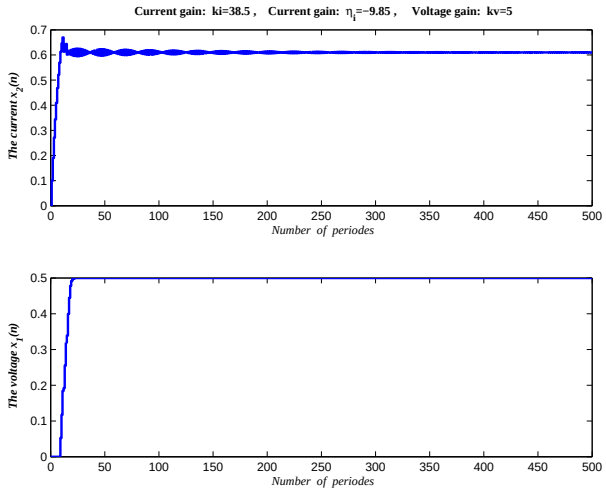


Figure 6: Evolution of the states under a Digital TDFC.

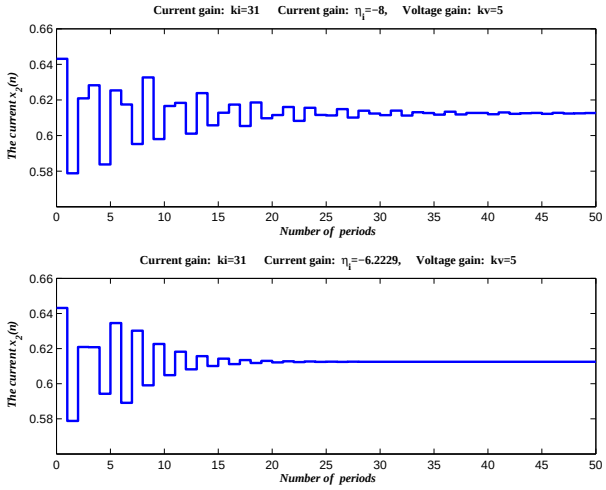


Figure 7: Evolution of the current under a Digital TDFC without and with optimized parameters.

periodic behaviors and black stands for chaotic motion. Brown stands for the $T$-periodic behavior and it confirms the triangular zone obtained theoretically. If we look at the horizontal line $\eta_i = 0$, we observe that the behavior

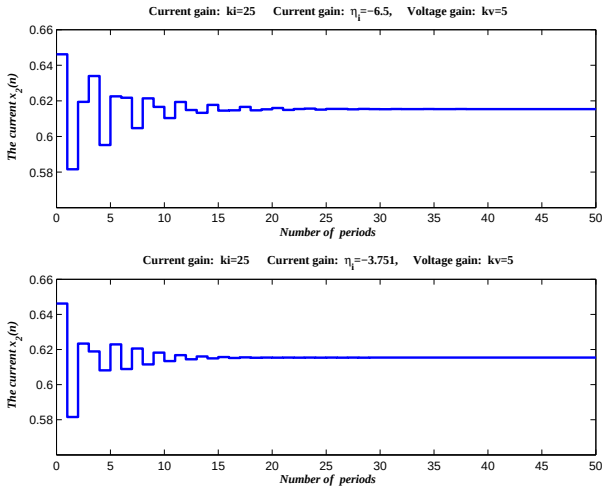


Figure 8: Evolution of the current under a Digital TDFC without and with optimized parameters (confirmation).

is exactly that obtained on Fig. 4 with red standing for $2T$-periodic behavior and so on. In Fig. 9 we also plot in dashed line the curve of optimal pairs. Although, one may intuitively choose a pair situated in the middle of the stability zone (*e.g.* results shown in Figs. 7 and 8) thinking to have faster response when situated far from the stability limits; we notice that the optimality curve is in fact and surprisingly very close to the upper limit of the stability zone.

### *3.4. Unpredicted Behavior: Coexistence of Attractors*

When exploring the optimality condition obtained in (55), we have chosen to start the simulation in the vicinity of the fixed point with the aim to observe the effect of the parameter choice and eliminate any other effects such as transients due to far initial conditions. It is worth noting that we have obtained a rather unpredictable behavior for some very particular pairs. We

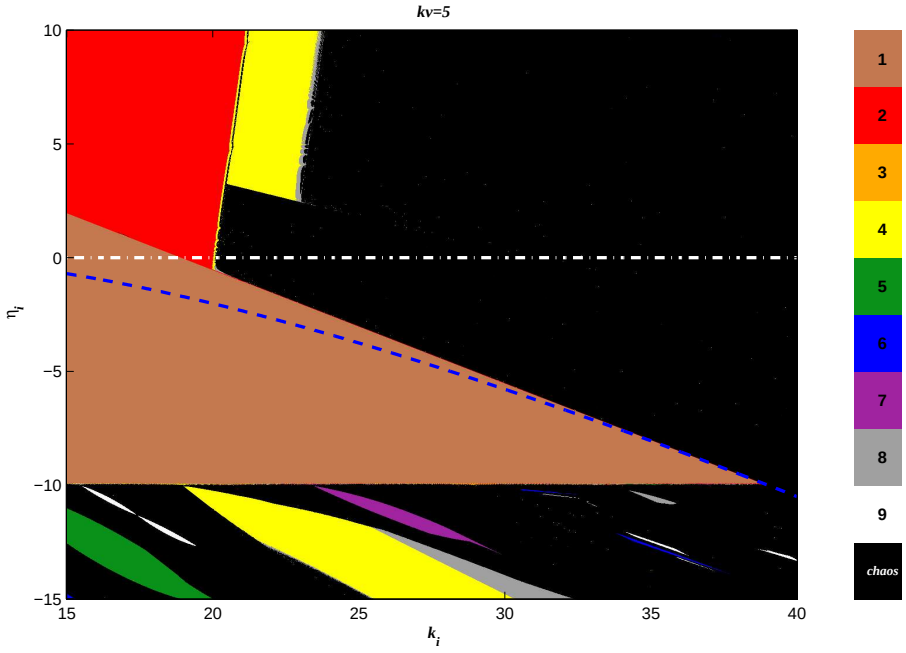


Figure 9: 2D-Bifurcation diagram of the converter behavior under the action of a Digital TDFC. Initial conditions simulations are selected at +5% of the fixed point values.

present in Fig. 10 the evolution of the current with $(k_i, \eta_i) = (31, -9)$. We notice that the current evolution is chaotic with values wandering within three different intervals (three piece chaotic attractor). Unlike the 2D-bifurcation diagram presented in Fig. 9 where simulations start at the origin of the state space, the 2D-bifurcation diagram presented in Fig. 11 is obtained by carrying simulations that start at +5% of the fixed point values. There, we have a slight difference in the region of $k_i = 31$. Indeed, chaotic behavior is obtained from pairs that according to the stability analysis, should give stable fixed point! We should point out here that this specific region changes slightly its shape according to the initial conditions and the value of $k_v$. To make an in depth investigation we plotted a bifurcation diagram with $\eta_i = -9.8$ using

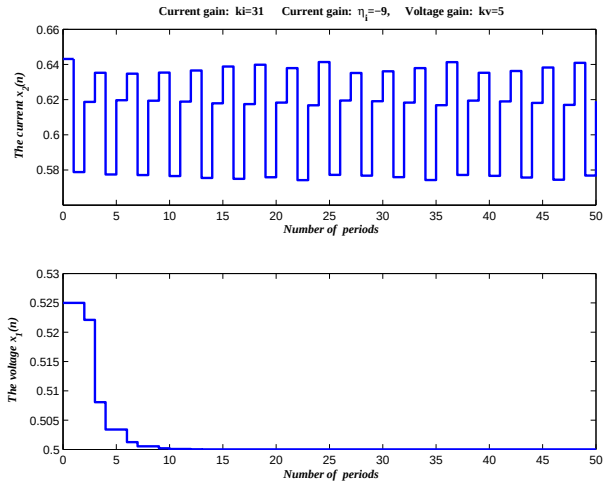


Figure 10: Evolution of the current $x_1[n]$ and the voltage $x_2[n]$ under a Digital TDFC with particular parameters. Initial conditions simulations are selected at the fixed point values.

simulations that start at +5% of the fixed point values. The diagram of Fig. 12 shows a chaotic attractor with three separate regions in the interval (29.3, 33.5) of the bifurcation parameter $k_i$. The sensitivity of the current evolution to initial condition implies here the coexistence of periodic motion and chaotic behavior. In Fig. 13, we present the basins of attraction of the fixed point (in brown) and of the chaotic attractor (in black) using some fixed parameters. We first note that the basins of attraction are intertwined. The separatrices are mainly vertical; making the basins independent of $x_3[n]$, except in some region where they have a different shape. Actually, in the regions where the basins of attraction are formed from vertical strips, we note that the duty cycles are both saturated either at zero $d_1 = d_2 = 0$ for lower values of initial conditions (call that region $\mathcal{R}_0$) or saturated at one $d_1 = d_2 = 1$ for higher values of initial conditions (call that region $\mathcal{R}_1$). The

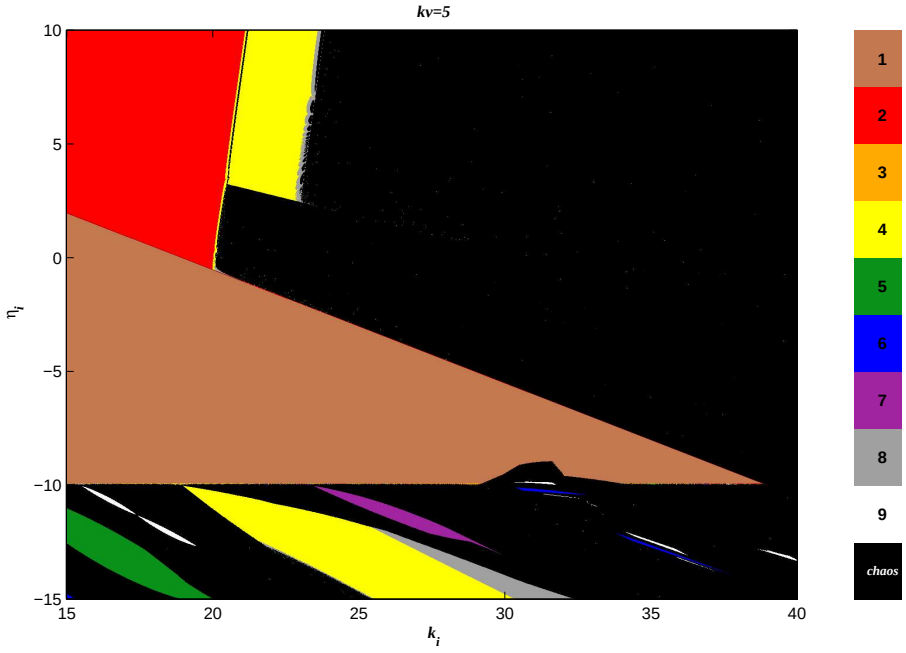


Figure 11: 2D-Bifurcation diagram of the converter behavior under the action of a Digital TDFC. Initial conditions simulations are selected at +5% of the fixed point values. White dashed line corresponds to the bifurcation 1D-diagram of Fig. 4(a). Blue dashed line corresponds to the optimum value of $\eta_i$ in terms of $k_i$.

boundaries of saturation of $d_1$ and $d_2$ are plotted in yellow and red respectively.

Now, when the system starts evolving in $\mathcal{R}_0$, it is attracted towards a virtual fixed point in $\mathcal{R}_1$ and vice-versa. The evolution of the current follows the line $\mathcal{L}_0 : x_3[n] = \frac{1}{1-\delta_L} x_2[n] - \frac{\delta_L}{1-\delta_L}$ in $\mathcal{R}_0$ (see the yellow circles and white asterisks). In $\mathcal{R}_1$ the evolution of the current follows the line $\mathcal{L}_1 : x_3[n] = \frac{1}{1-\delta_L} x_2[n]$ (see the cyan triangles and magenta diamonds). Eventually, the evolution should reach a region delimited by the duty cycle saturation lines and the lines $\mathcal{L}_0$ and $\mathcal{L}_1$ (call that region $\mathcal{R}_{fp}$). Once the trajectories are

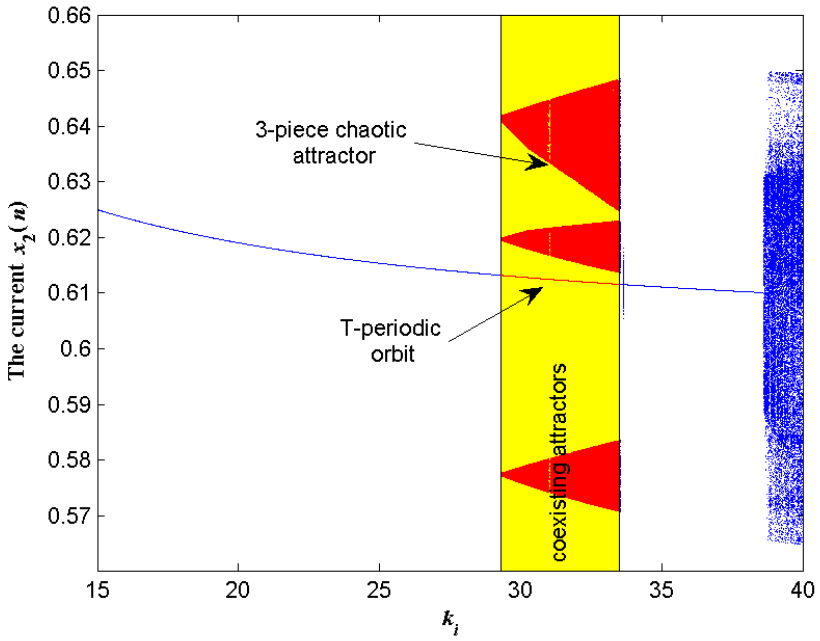


Figure 12: Bifurcation diagram showing coexistence of chaotic attractor and periodic behavior under the action of a Digital TDFC. Three piece chaotic attractor coexists with $T$-periodic orbit within the range (29.3, 33.5) of the bifurcation parameter $k_i$.

in $\mathcal{R}_{fp}$, the system will either converge to the fixed point or to the three-regions chaotic attractor. In Fig. 14, we present a zoom of the region $\mathcal{R}_{fp}$, there we observe that trajectories attracted by the fixed point will reach it while spiraling around it since we can check that the eigenvalues associated to the fixed point are complex conjugate. Now, in absence of saturation of the duty cycles, the fixed point is globally attractive. However, in presence of the saturation, points which are still far from the fixed point, *i.e,* next to the boundaries of the region $\mathcal{R}_{fp}$, might be attracted to another virtual fixed point following different trajectories. This is the key point of the problem. If

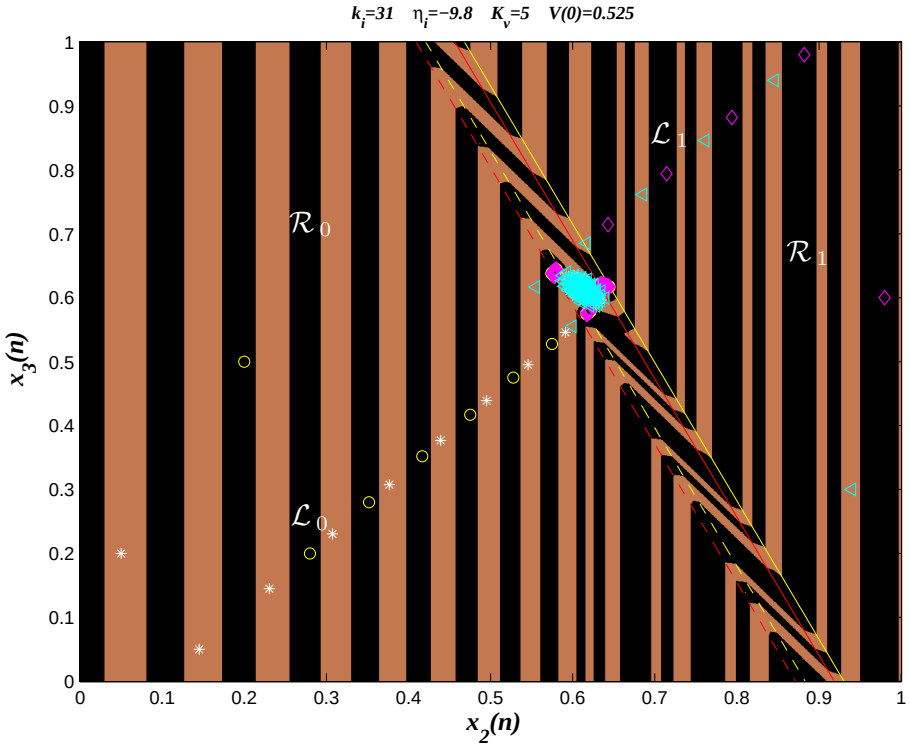


Figure 13: Riddled basins of attraction of the coexisting attractor and the fixed point. In brown, the basin of attraction of the fixed point and in black the basin of attraction of the there-regions chaotic attractor. In white asterisks and cyan triangles we present two system trajectories converging to the fixed point and initiated at $\mathcal{R}_0$ and $\mathcal{R}_1$ respectively. In yellow circles and magenta diamonds we present two system trajectories converging to the chaotic attractor and initiated at $\mathcal{R}_0$ and $\mathcal{R}_1$ respectively.

a trajectory gets close to the fixed point such that its future evolution does not leave the non-saturation region then it converges to the fixed point. On the other hand, if a trajectory approaches the fixed point but still relatively far so that its future steps are outside the non-saturation region then it will go farther by the effect of the virtual fixed points but cannot leave the region $\mathcal{R}_{fp}$. That's how a new chaotic attractor has been created.

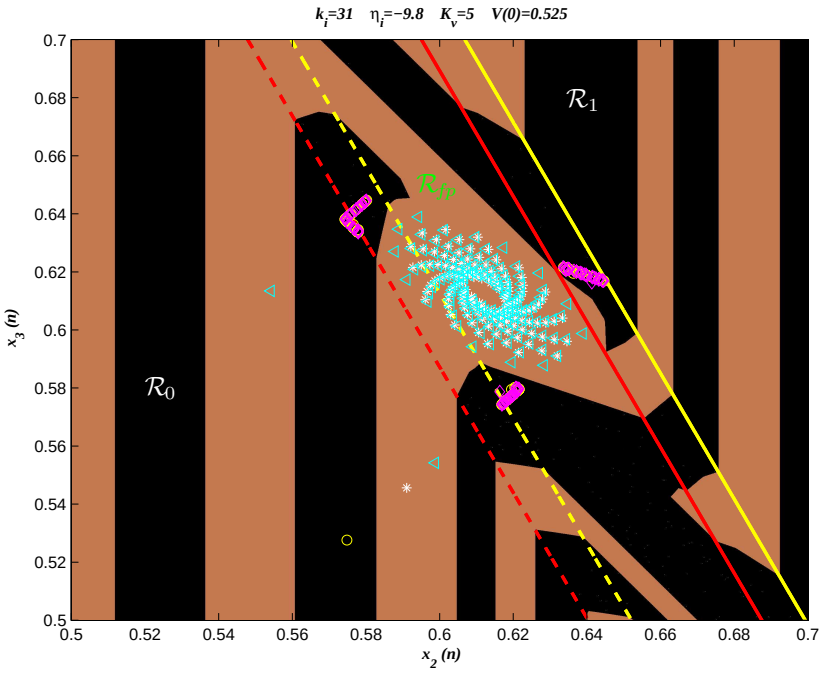


Figure 14: Zoom about the fixed point and the coexisting chaotic attractor. In brown, the basin of attraction of the fixed point and in black the basin of attraction of the there-regions chaotic attractor. In white asterisks and cyan triangles we present two system trajectories converging to the fixed point and initiated at $\mathcal{R}_0$ and $\mathcal{R}_1$ respectively. In yellow circles and magenta diamonds we present two system trajectories converging to the chaotic attractor and initiated at $\mathcal{R}_0$ and $\mathcal{R}_1$ respectively.

## Conclusion

In this paper, we have presented two discrete models of a two-cell DC-DC buck converter, starting from the most complete and complicated one to the approximated and simplest one. The advantage of the complex one is to reflect with a great fairness the behavior of the real system, though it cannot be processed from an analytical point of view. On the contrary, the

advantage of the simple and approximated model is that it can be handled analytically with the aim to design controller to harness any abnormal behavior that can be exhibited by the converter. The obtained models have been then simulated numerically to predict behaviors of the converter. The simplicity of its architecture does not prevent it from having a rich spectrum of complex dynamical behavior. The most amazing among these behaviors is the chaotic one which is usually classified as undesirable in power electronics. The purpose of the present work has been to design a feedback control signal that help to suppress the chaotic behavior with the aim to ameliorate the performance of the converter and to enlarge the domain of its application. Here, we have presented the TDFC controller. The normal periodic behavior has been stabilized in some parameter space where chaotic behavior has been observed. The controller presents several advantages. The first is that it still has a simple expression to be implemented physically. The second advantage is the speed of its action if the time delayed feedback gain $\eta_i$ is optimized and the third advantage is its non-invasiveness since the TDFC term vanishes when the system reaches the period-one behavior. Of course, we do not claim to present the perfect solution to the problem in question, albeit several advantages have been cited. In fact, from a control theory point of view, our analysis has neglected the duty cycle saturation which requires an in depth analysis to guarantee the stability and to avoid any bad surprise in the real operation of the converter like the coexistence of attractors discovered by numerical simulations. This constitutes a first point that we have already started to investigate in order to present a complete theoretical analysis about this issue. This complete study together with an experimental

validation will be the subject of a future work.

## Acknowledgments

This work is done within a Tunisian-Spanish cooperation framework under grant A/021698/08. Spanish *Ministerio de Educación e Innovación* under grant DPI2010-16481 is acknowledged.

## References

[1] Bose B. K (Ed.), Modern Power Electronics: Evolution, Technology, and Applications, New York: IEEE Press, 1992.

[2] Rashid M. H. (Ed.), Power Electronics Handbook, Second Edition, Academic Press, 2006

[3] Verghese, G.C., Elbuluk, M., and Kassakian, J.G., *A general approach to sample-data modeling for power electronic circuits*, IEEE Trans. Power Elect. 1(2) (1986), pp. 76-89.

[4] Fossas, E. Olivar, G., *Study of Chaos in the Buck converter*, IEEE Trans. Circuits Syst. I 43(1) (1996), pp. 13-25.

[5] Deane, J.H.B. and Hamill, D.C., *Instability, subharmonics and chaos in power electronic systems*, IEEE Trans. Power Elect. 5(3) (1992), 260-268.

[6] Tse, C.K., *Chaos from a Buck Switching Regulator Operating in Discontinuous Mode*, Int. J. Circuit Th. Appls. (4) (1994), 263-278.

[7] Tse, C.K., *Flip Bifurcation and Chaos in Three-state Boost Switching Regulators*, IEEE Trans. Circuits Syst. I 41(1) (1994), pp. 16-23.

[8] Banerjee S. and Verghese G. C. (Edts.), *Nonlinear Phenomena in Power Electronics*, (New York), IEEE Press, 2001.

[9] El Aroudi, A., Debbat, M., Olivar, G., Benadero, L., Toribio, E., and Giral, R., *Bifurcations in DC-DC Switching Converters, Review of Methods and Applications*, Int. J. Bifurcations and Chaos 15(5) (2005), pp. 1549-1578.

[10] Zhusubaliyev, Z. T., Soukhoterin E. A., Mosekilde E., *Border collision bifurcations and chaotic oscillations in a piecewise smooth dynamical system*, Int. J. Bifurcation & Chaos 11(12) (2001), pp. 152-163

[11] Zhusubaliyev, Z. T., Mosekilde E., *Bifurcations and chaos in piece-wise smooth dynamical systems,* World scientific series on nonlinear science. Series A, vol.44.

[12] Zhusubaliyev Z. T, Mosekilde E., *Birth of bilayered torus and torus breakdown in a piecewise-smooth dynamical system Physics Letters A*, Volume 351, Issue 3, 27 February 2006, pp. 167-174.

[13] Chen Y., Tse C.K., Qiu S-S., Lindenmuller L. and Schwarz W., *Coexisting Fast-Scale and Slow-Scale Instability in Current-Mode Controlled DC/DC Converters: Analysis, Simulation and Experimental Results*, IEEE Transactions on Circuits and Systems I, 55, 10, (2008), pp. 3335-3348.

[14] Colombo A., Lamiani P., Benadero L., and di Bernardo M., *Two-Parameter Bifurcation Analysis of the Buck Converter*, SIAM J. Applied Dynamical Systems, 8, 4 (2009), pp. 1507-1522.

[15] Benadero, L., El Aroudi, A., Olivar, G., Toribio, E., and Gómez, E. *Tow-dimensional bifurcation diagrams background pattern of fundamental DC-DC converters with PWM control*, Int. J. Bifurcation & Chaos 13(2) (2003), 427-451.

[16] K. Åström and B. Wittenmark, *Computer-Controlled Systems. Theory and Design*, 2nd ed, Prentice-Hall, 1990.

[17] Kuo, B. C., *Digital Control Systems*, Birkhäuser, Boston, 2003.

[18] Robert, B. and El Aroudi, A., *Discrete Time Model of a Multi-Cell DC/DC Converter, Non Linear Approach*, Mathematics and Computers in Simulation 71(4-6) (2006), pp-310-319.

[19] El Aroudi, A., Robert, B., Cid-Pastor, A., Martínez-Salamero, L., *Modelling and Design Rules of a Two-Cell Buck Converter Under a Digital PWM Controller. IEEE Transactions on Power Electronics*, 23, 2 (2008), pp. 859-870.

[20] Meynard, T. A., Fadel, M., and Aouda, N., *Modeling of Mutlilevel Converters*, IEEE Trans. on Ind. Elect 44(3) (1997), pp-356-364.

[21] Yousefzadeh V., Alarcón E., Maksimovic D, *Three-Level Buck Converter for Envelope Tracking in RF Power Amplifiers*, APEC'05- IEEE Applied Power Electronics Conference (2005), Austin, Texas.

[22] Schöll, E. and Schuster H. G., Handbook of Chaos Control, Wiley–VCH, 2005.

[23] Andrievskii, B. R., and Fradkov, A. L., *Control of Chaos, Methods and Applications. I. Methods*, Automation and Remote Control 64(5), (2003), pp-673-713.

[24] Pyragas K., *Control of Chaos via an Unstable Delayed Feedback Controller*, Physical Reviews Letters, 86, (11) (2001), pp. 2265-2268.

[25] Batlle, C., Fossas E., and Olivar, G., *Stabilization of periodic orbits of the buck converter by time-delayed feedback*, Int. J. Circuit Th. Appls 27(5) (1997), pp. 617-631.

[26] Bouzahir H., El Guezar F., El Aroudi A., and Ueta T., *Partial Time Delayed Feedback Control of Chaos in a Switched System*, 3rd International Symposium on Communications, Control, and Signal Processing, (2008), Hotel Le Meridien, St. Julians, Malta.

[27] Iu, H.H.C. and Robert, B., *Control of chaos in a PWM current-mode H-bridge inverter using time-delayed feedback*, IEEE Trans. Circuits Syst. I 50 (8) (2003), pp. 1125-1129.

[28] Robert, B.G.M., Feki, M., Iu, H.H.C., *Control of PWM Inverter Using a Proportional Plus Extended Time-Delayed Feedback Controller*, Int. J. Bifurcation & Chaos 16(1) (2006), pp. 113-128.

[29] Bai X.-M., Li H.-M., and Yang X.-S., *Some results on cascade discrete-time systems*, Discrete Dynamics in Nature and Society, no. DOI 10.1155/DDNS/2006/14631, (2006), pp. 1-8.

[30] Feki, M., El Aroudi, A. and Robert, B G M., *Multi-cell DC/DC converter: Modeling, analysis and control*, Internal report of a Tunisian-Spanish PCI cooperation project No A/6828/06 (2007).